Version of Record: https://www.sciencedirect.com/science/article/pii/S1540748922002966
Manuscript_0058009c6b3df4a20e6a04d3656e6dbe

Bay capping via acetylene addition to polycyclic aromatic hydrocarbons: Mechanism and kinetics

Lotefa Binta Tuli[a], Alexander M. Mebel[a,*], Michael Frenklach[b]

[a]*Department of Chemistry and Biochemistry, Florida International University, Miami, Florida, 33199, USA*
[b]*Department of Mechanical Engineering, University of California at Berkeley, Berkeley, California, 94720-1740, USA*

Abstract

The bay-capping mechanism on PAH armchair edges and the kinetics of acetylene addition to 6-6-5 and 5-6-5 bays have been explored by *ab initio*/RRKM-ME calculations. The bays on the edges were modeled by $C_{21}H_{11}$ and $C_{20}H_9$ radicals produced by H abstractions from 7*H*-benzo[*c*]cyclopenta[*e*]pyrene and dicyclopenta[*cf*]pyrene. The $C_{20}H_9 + C_2H_2$ reaction is shown to have a low entrance barrier and to rapidly form the capped product, indaceno[2,1,8,7-*cdefg*]pyrene, along with ethynyl substituted dicyclopenta[*cf*]pyrene at temperatures above 1400 K. The reactivity of $C_{21}H_{11}$ is shown to be governed by the location of the unpaired electron; the π radical R1 formed by H abstraction from the CH_2 group in 7*H*-benzo[*c*]cyclopenta[*e*]pyrene reacts with C_2H_2 very slowly owing to a high entrance barrier, with the bay-capping rate constant approaching 10^{-16} cm^3 $molecule^{-1}$ s^{-1} only at temperatures above 2000 K. This result reaffirms that the growth of π aryl radicals via acetylene addition is inefficient and reflects the generally low reactivity of such radicals where the spin density is highly delocalized over the entire polyaromatic system. Alternatively, the σ $C_{21}H_{11}$ radical R2 produced by H abstraction from the five-membered ring at the bay rapidly reacts with C_2H_2 forming the bay-capped product, with the rate constant on the order of 10^{-12} cm^3 $molecule^{-1}$ s^{-1} at $T \geq 1500$ K. Rate constants for the capping reactions at the 6-6-5 and 5-6-5 bays are compared with those at the 6-0-6, 6-6-6, and 6-5-6 bays. The site-specific bay-capping rate constants have been utilized in kMC simulations of the PAH growth and the results showed measurable differences when the 6-6-5 and 5-6-5 bay-capping reactions are taken into account, including an increase of the growth rate and the formation of closed-shell PAH and a rise of the number of embedded five-membered rings accompanied with a slight decrease of their overall amount.

Keywords: PAH growth; Bay capping; Hydrogen-Abstraction/C_2H_2-Addition (HACA); Reaction mechanism; Soot

*Corresponding author.

© 2022 published by Elsevier. This manuscript is made available under the Elsevier user license
https://www.elsevier.com/open-access/userlicense/1.0/

1. Introduction

Hydrogen-Abstraction/C_2H_2-Addition (HACA) mechanism put forward by Frenklach and co-workers [1,2] remains the most generally accepted mechanism for the growth of polycyclic aromatic hydrocarbons (PAHs). HACA successfully describes the PAH growth in various flames by kinetic models [3-10] and has been confirmed by molecular beam experiments in pyrolytic reactors, in particular, for the formation of naphthalene from benzene [11-13] and for the growth of an extra six-membered ring on armchair PAH edges, such as in the formation of phenanthrene from biphenyl, pyrene from phenanthrene, and corannulene from fluoranthene [14-17]. The acetylene addition reactions on armchair edges in these systems can be characterized as bay capping resulting in the formation of an additional six-membered ring and a change of the PAH edge to zigzag.

The bay-capping mechanism is similar in all systems studied so far [10,14-17] and involves typical steps of C_2H_2 addition, the ring closure, and an H atom loss competing with a hydrogen atom loss immediately after the acetylene addition leading to the formation of an ethynyl substituted reactant. However, the entrance barrier and the reaction enthalpies for the channels leading to the formation of the bay-capped product and the ethynyl substituted molecule may vary in wide margins. These details are governed by the bay structure, namely, and of primary interest to the present study, by the presence and combination of six- and five-membered constituent rings.

The bay sites considered in the present study are shown in Fig. 1. They include two six-membered rings connected by (a) a C-C bond, 6-0-6 (biphenyl) or (b) a central six-membered ring, 6-6-6 (phenanthrene), (c) two six-membered rings connected by a central five-membered ring, 6-5-6 (fluoranthene and benzo[*ghi*]fluoranthene), (d) six- and five-membered rings connected by a central six-membered ring, 6-6-5, and (e) two five-membered rings connected by a central six-membered ring, 5-6-5. We do not consider structures with two adjacent five-membered rings since those are energetically unfavorable and hence uncommon in PAH [18].

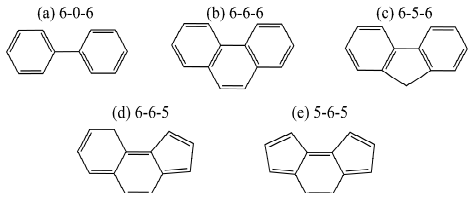

Fig. 1. Possible structures of PAH bay sites.

Structure (b), 6-6-6, represents the armchair edge and its growth through capping was the first application of HACA [1]. Structure (c), 6-5-6, occurs in embedded five-membered ring migration [19] and its capping numerically simulated PAH curving [20,21]. The omnipresence of five-membered rings in the evolving PAH structure was one of the predictions of HACA [1] and now has been firmly established experimentally [22,23] and computationally [20,24,25]. It is, therefore, naturally to ask if other bay structures composed of six- and five-membered rings could occur in PAH growth and whether capping of such sites would contribute to the growth.

The present study explores these questions by examining capping by acetylene addition of bay sites (d), 6-6-5, and (e), 5-6-5, which has not been investigated to our knowledge. Sites 6-6-5 and 5-6-5 were represented by radicals formed by H abstractions from the 7*H*-benzo[*c*]cyclopenta[*e*]pyrene $C_{21}H_{12}$ and dicyclopenta[*cf*]pyrene $C_{20}H_{10}$ molecules. The choice of these radicals for simulating the 6-6-5 and 5-6-5 bay sites, respectively, is justified by the fact that the models should generally describe PAH edges more realistically when at least one layer of aromatic rings is included under the bay site. We calculated potential energy surfaces (PES) for acetylene addition to these sites and evaluated their rate constants. These results were compared to those of sites 6-0-6, 6-6-6, and 6-5-6 and their effect on PAH growth was tested in kinetic Monte Carlo (kMC) simulations.

2. Calculation methods

Density functional theory (DFT) B3LYP [26,27] calculations with the 6-311G(d,p) basis set were carried out for geometry optimization of all species on the considered $C_{22}H_{11}$ and $C_{23}H_{13}$ potential energy surfaces (PES) accessed by the bay-capping reactions of the $C_{20}H_9$ and $C_{21}H_{11}$ radicals with acetylene, as well as for H abstractions from the $C_{21}H_{12}$ molecule by H atoms. Vibrational frequencies for all stationary structures were calculated at the same B3LYP/6-311G(d,p) level of theory and the computed frequencies were utilized for the evaluation of zero-point vibrational energy (ZPE) corrections and in rate constant calculations. Single-point energies were refined using the standard composite model chemistry G3(MP2,CC) approach [28,29], in which a basis set correction obtained by MP2 calculations with the G3Large and 6-31G(d) basis sets is added to the CCSD(T)/6-31G(d) energy along with ZPE. All B3LYP calculations were carried out using the Gaussian 16 program package [30], whereas the CCSD(T) and MP2 calculations were performed with the MOLPRO 2021 code [31].

Temperature- and pressure-dependent rate constants in the temperature range of 500-2500 K and in the pressure range of 0.01-100 atm were

computed employing the RRKM-ME approach [32] as implemented in the MESS code [33,34], generally within the rigid rotor-harmonic oscillator approximation (RRHO). Internal rotations corresponding to low-frequency vibrational modes were treated as hindered rotors and their internal rotational potentials were evaluated using B3LYP/6-31G(d) PES scans along the corresponding torsional angles. The computed internal rotational potentials allowed us to ensure that the lowest in energy conformer is chosen for the calculations of the reaction kinetics, e.g., for the initial adducts. The Lennard-Jones parameters ε and σ required for RRKM-ME calculations were estimated depending on the molecular mass of the intermediates involved in the reaction as proposed by Wang and Frenklach [35] and the parameters for the N_2 bath gas were taken from Vishnyakov et al. [36,37]. The "exponential down" model [38] was used to treat the collisional energy transfer in ME, with the temperature dependence of the range parameter α for the deactivating wing of the energy transfer function expressed as $\alpha(T) = \alpha_{300}(T/300\ \mathrm{K})^n$. The values of $n = 0.62$ and $\alpha_{300} = 424\ \mathrm{cm}^{-1}$ in this expression were earlier derived by Jasper from classical trajectory calculations [39,40] and were systematically used by us in the studies of C_2H_2 addition reactions to various PAH radicals [10,15-17,40,41].

3. Results and discussion

3.1 Potential energy surfaces for bay capping

We first consider the bay-capping reaction between two five-membered rings attached to a central six-membered ring as in the dicyclopentapyrene molecule, $C_{20}H_{10}$. The potential energy diagram for acetylene addition to the $C_{20}H_9$ radical formed after H atom from a five-membered ring at the bay position is shown in Fig. 2.

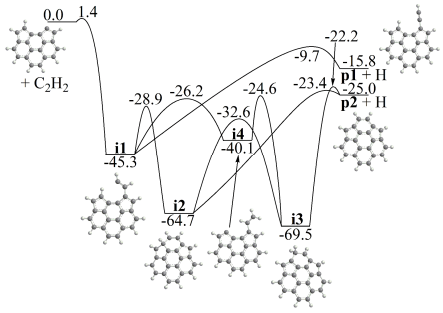

Fig. 2. Potential energy diagram for the $C_{20}H_9 + C_2H_2$ reaction. Relative energies are given in kcal/mol.

The $C_{20}H_9$ radical has a σ character and easily reacts with C_2H_2 overcoming a barrier of only 1.4 kcal/mol. The acetylene addition results in the initial intermediate **i1**, which can either decompose to the ethynyldicyclopentapyrene product **p1** via H loss from the α carbon atom in the side chain or undergo a six-membered ring closure—the bay-capping process. The ring closure may occur immediately (**i1** $\rightarrow$ **i2**) or be preceded by 1,6-H migration from the five-membered ring to the β C atom in the side chain (**i1** $\rightarrow$ **i4**). The six-membered closure in **i4** and 1,2-H shift in **i2** both lead to the same intermediate **i3**, which in turn can eliminate an extra hydrogen atom forming the final bay-capped product $C_{22}H_{10}$ **p2**, indaceno[2,1,8,7-*cdefg*]pyrene. The **i1** $\rightarrow$ **i2** $\rightarrow$ **i3** pathway appears to be preferential as compared with **i1** $\rightarrow$ **i4** $\rightarrow$ **i3** due to the lower-lying transition states (TS). Also, **i2** can decompose to **p2** + H directly. The **p1** + H and **p2** + H products respectively reside 15.8 and 25.0 kcal/mol below the reactants with the corresponding TS located at -9.7 and -23.4/-22.2 kcal/mol with respect to $C_{20}H_9 + C_2H_2$. For comparison, the bay-capping process involving the 4-phenanthrenyl radical [10,16], i.e., in the bay (armchair edge) formed by three six-membered rings, the C_2H_2 addition reaction energies to produce the 4-ethynylphenanthrene and pyrene products are -4.0 and -58.8 kcal/mol, meaning that bay capping in 4-phenanthrenyl is much more favorable thermodynamically than in $C_{20}H_9$. The difference can be attributed to the fact that because of the presence of two five-membered rings in near vicinity from one another, indaceno[2,1,8,7-*cdefg*]pyrene is not a planar molecule and thus the aromatic stabilization is partially lost. It is also interesting to compare the bay -capping reaction energy in $C_{20}H_9$ with those in 7-fluoranthenyl ($C_{16}H_9$) forming benzo[*ghi*]fluoranthene and in benzo[*ghi*]fluoranthen-5-yl ($C_{18}H_9$) producing corannulene, -46.6 and -35.9 kcal/mol, respectively, both including only one five-membered ring [17]. Here, the bay-capping process occurs between two six-membered rings connected to a central five-membered ring but the product is planar for 7-fluoranthenyl and non-planar, though highly symmetric corannulene for benzo[*ghi*]fluoranthen-5-yl. In the meantime, the reaction rate is likely to be controlled not by the thermodynamical preference of the bay-capped product but by the height of the entrance barrier for C_2H_2 addition, which is the highest for 4-phenanthrenyl (4.7 kcal/mol) followed by those for benzo[*ghi*]fluoranthen-5-yl (4.4 kcal/mol), 7-fluoranthenyl (2.3 kcal/mol), and $C_{20}H_9$ here (only 1.4 kcal/mol), and the bay-capping branching fraction vs. the formation of the ethynyl-substituted product.

Next, we look at bay capping between a six- and a five-membered ring connected to a central six-membered ring as in $C_{21}H_{11}$ radicals produced by H abstractions from $C_{21}H_{12}$ (Fig. 3). The $C_{21}H_{12}$ molecule features a CH_2 group on the six-membered ring in the bay area. The C-H bond in this group is much weaker than the regular aromatic C-H bond

and therefore it is easier to abstract an H atom from CH_2 than from the five-membered ring on the other side of the bay. For instance, the reaction energies of $C_{21}H_{12} + H \rightarrow C_{21}H_{11} + H_2$ are calculated to be -43.9 and 12.2 kcal/mol when the radicals R1 and R2 are formed as a result of H abstraction from the CH_2 group and the five-membered ring, respectively. The difference in the barrier heights is not that large but still significant, 2.9 vs. 18.8 kcal/mol. The R1 isomer of $C_{21}H_{11}$ is 56.1 kcal/mol more stable than R2. R1 is a π radical with the spin density delocalized over the entire polyaromatic system. The calculated PES (see Fig. S1 for a more detailed potential energy diagram) indicates that the reaction of R1 with acetylene is unfavorable. The addition of C_2H_2 to the π radical site in the six-membered ring at the bay exhibits a high barrier of 27.5 kcal/mol and leads to an endothermic initial complex **i1**. The H loss from the side chain in **i1** which normally competes with bay capping is highly endothermic here with the product lying 47.8 kcal/mol above R1 + C_2H_2.

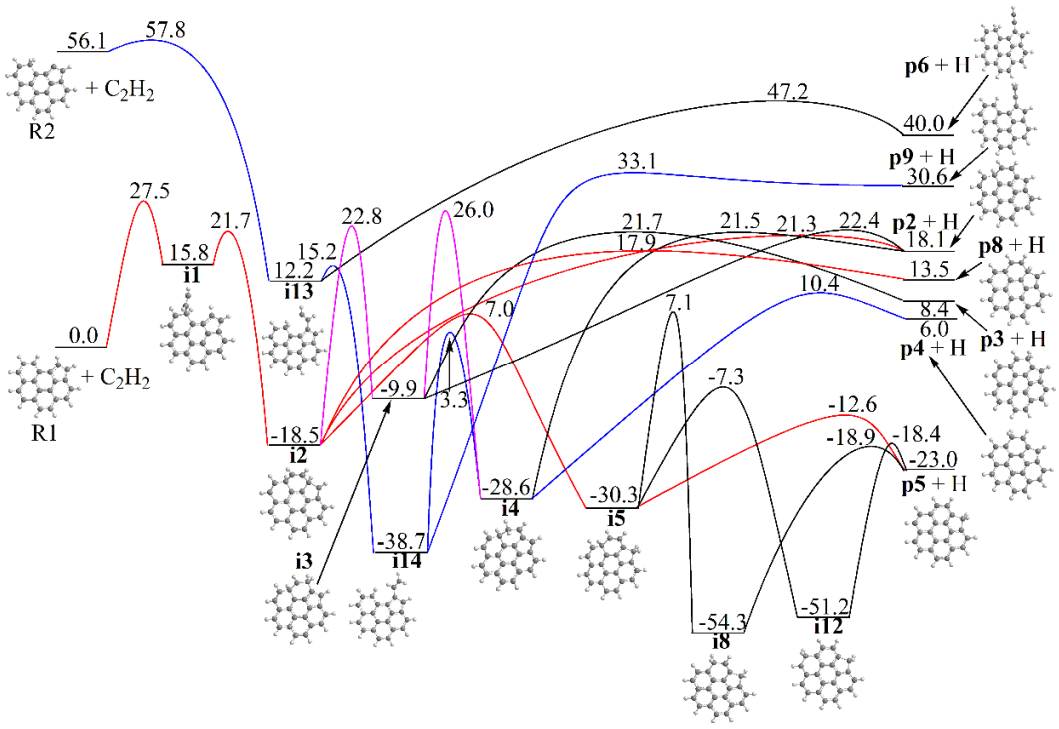

Fig. 3. Potential energy diagram for the $C_{21}H_{11} + C_2H_2$ reaction. Relative energies are given in kcal/mol.

Alternatively, the six-membered ring closure in **i1** is facile producing **i2** over a barrier of 5.9 kcal/mol. The intermediate **i2** can either lose an H atom to form the bay-capped products **p2** or **p8** endothermic by 18.1 and 13.5 kcal/mol, respectively, or feature a 1,2-H shift in the five-membered ring leading to **i3**, which then dissociates to a much more favorable $C_{23}H_{12}$ product **p5**, 7*H*-benzo[*ghi*]cyclopenta[*pqr*]perylene, exothermic by 23.0 kcal/mol. While the energies of the bay-capping reactions occurring via C_2H_2 additions to the π radical $C_{21}H_{11}$ R1 and the σ radical $C_{20}H_9$ are similar, the π radical reaction is hindered by a very high entrance barrier making it non-competitive, as will be shown in the kinetics subsection below.

If a σ radical R2 is produced by less favorable H abstraction from the five-membered ring, this radical can react with acetylene much easier. The barrier for the C_2H_2 addition is only 1.7 kcal/mol and the initial complex **i13** formed resides 43.9 kcal/mol below the reactants. **i13** can either lose an H atom from the acetylene moiety forming **p6** exothermic by 16.1 kcal/mol or undergo a 1,6-H shift from the CH_2 group in the six-membered ring to the terminal C atom of the side chain. The H migration barrier is as low as 3.0 kcal/mol leading to **i14** which resides a deep potential well. The latter intermediate can dissociate to an arene-substituted allene **p9** by H loss from the side chain or be subjected to the six-membered ring closure at the bay producing **i4**. Finally, the latter can split an H atom to form the bay-capped products, preferentially, 5*H*-benzo[*ghi*]cyclopenta[*pqr*]perylene **p4** (at -50.1 kcal/mol relative to R2 + C_2H_2) or, less likely, **p2** (at -38.0 kcal/mol). Thus, according to the calculated

PES, the bay closure process via C_2H_2 to the σ radical R2 is anticipated to be fast. It is also worth noting that the two reaction pathways initiating from R1 and R2 are linked by H migrations in **i2** and **i4** via the intermediate **i3**, but the corresponding barriers are high.

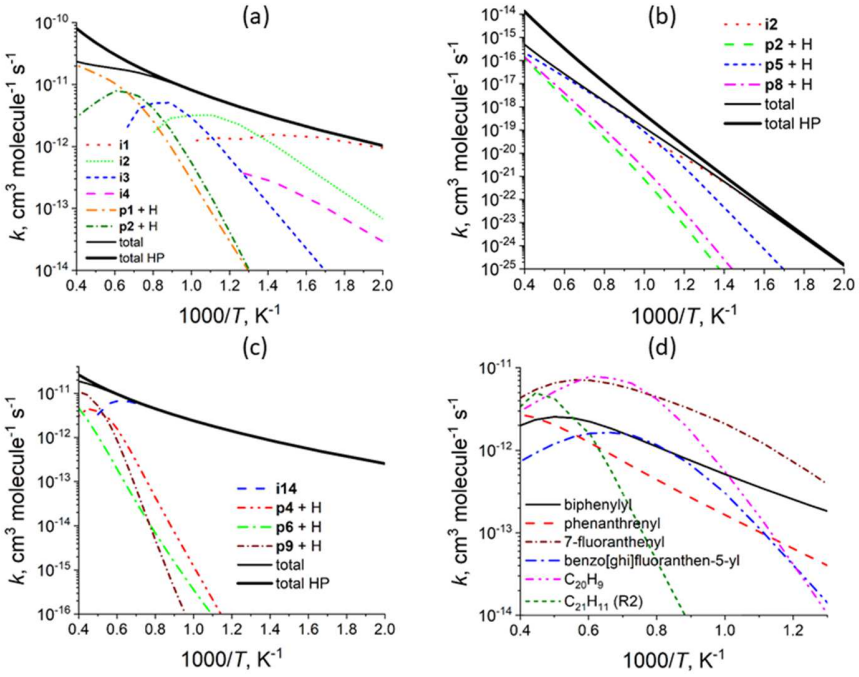

Fig. 4. Total and individual channel rate constants calculated at 1 atm: (a) $C_{20}H_9 + C_2H_2$; (b) $C_{21}H_{11}$ (R1) + C_2H_2; (c) $C_{21}H_{11}$ (R2) + C_2H_2; (d) comparison of rate constants of bay-capping reactions on various sites.

3.2 Bay-capping kinetics

The total and individual channel rate constants for the $C_{20}H_9 + C_2H_2$ reaction calculated at 1 atm are illustrated in Fig. 4(a), whereas the overall set of rate constants in this reaction system including those for reverse reaction and product branching ratios at various temperatures and pressures can be found in Supplementary material. The reaction is predicted to be fast, with the high pressure limit (HP) rate constant growing from 1.0×10^{-12} to 8.0×10^{-11} cm^3 molecule^{-1} s^{-1} in the 500-2500 temperature range. The total rate constant at 1 atm is close to the HP limit up to ~1300 K and then falls off; at 2500 K $k_{1\ atm}$ is a factor of 3.4 lower than k_{HP}. At low temperatures, the reaction preferentially forms collisional stabilized intermediates, **i1** at 500-700 K, **i2** up to 1000 K, and **i3** up to 1200 K, whereas at higher temperatures **p1** and **p2** becomes predominant and then, above 1500 K, exclusive products. The branching ratio of **p2** somewhat exceeds that of **p1** up to 1500 K, whereas at higher temperatures the yield of **p1** is predicted to be higher due to the entropic preference of the immediate H loss following acetylene addition. Nevertheless, the bay-capping reaction channel producing indaceno[2,1,8,7-*cdefg*]pyrene **p2** is fast, with the rate constant maximizing at 6-8×10^{-12} cm^3 molecule^{-1} s^{-1} in the 1400-1800 K temperature range. Interestingly, the reverse **p1** + H reaction (0.7-1.4×10^{-11} cm^3 molecule^{-1} s^{-1}) nearly equally branches between the formation of the reactants and **p2** + H in this temperature interval. The reverse **p2** + H reaction is predicted to be a factor of 3-3.6 faster than $C_{20}H_9 + C_2H_2 \rightarrow$ **p2** + H and to produce the initial reactants and **p1** + H with similar yields. Thus, an equilibrium may be established between bay capping in $C_{20}H_9$ and desorption of acetylene from the edge of indaceno[2,1,8,7-*cdefg*]pyrene.

The $C_{21}H_{11}$ (R1) + C_2H_2 reaction of acetylene addition to a π radical is predicted to be very slow (Fig. 4b). The prevailing reaction channel at temperatures of 1000 K and above is the formation of the bay-capped product 7*H*-benzo[*ghi*]cyclopenta[*pqr*]perylene **p5**, although at high temperatures the yields of less thermodynamically stable **p2** and **p8** also become significant. Nevertheless, the total rate constant in the 1400-1800 K range is only 5×10^{-18}–5×10^{-17} cm^3 molecule^{-1} s^{-1} meaning that the bay-capping process via acetylene addition to a π radical is not expected

to play a significant role in PAH growth on the edges. In principle, this reaction can be enhanced if the R1 radical produced by highly exothermic H abstraction from $C_{21}H_{12}$ releasing 43.9 kcal/mol remains "hot" and does not equilibrate before it encounters a C_2H_2 molecule. This may happen at low pressures and high acetylene concentrations. However, a study of the energy distribution in R1 after H abstraction and the evaluation of the rate constant of energized R1 reacting with C_2H_2 is a complex task requiring a careful consideration, which is beyond the scope of the present paper.

Alternatively, the R2 + C_2H_2 reaction is fast (Fig. 4c), with the HP limit rate constant of 2.6×10^{-13}–2.6×10^{-11} cm^3 molecule^{-1} s^{-1} at T = 500-2500 K. The total rate constant at 1 atm is close to the HP limit; the fall-off difference reaches a factor of 1.4 at 2500 K. The formation of collisionally stabilized **i14** prevails up to 1800 K and at higher temperatures the major products are 5*H*-benzo[*ghi*]cyclopenta[*pqr*]perylene **p4** and arene-substituted allene **p9**. In the 1400-1800 K temperature range, the **i14** intermediate predominantly dissociates to the bay-capped product **p4** with the unimolecular rate constant of 4×10^{4}-2.3×10^{6} s^{-1}. The reverse **p9** + H reaction rapidly produces **i14** or **p4** + H, whereas the **p4** + H reaction results in H-assisted isomerization to the most thermodynamically favorable product **p5** with the rate constant as high as $1.1\text{-}1.7\times10^{-10}$ cm^3 molecule^{-1} s^{-1}. We can conclude therefore that the bay-capping process involving acetylene addition to the σ radical R2 is an efficient process. However, the probability that the R2 radical is produced by H abstraction from $C_{21}H_{12}$ molecule is low. The calculated rate constant for H abstraction by H from $C_{21}H_{12}$ to form the π radical R1 is 6.2×10^{-11}–1.2×10^{-10} cm^3 molecule^{-1} s^{-1} at T = 1400-1800 K, whereas that to form the σ radical R2 is 2-3 orders of magnitude lower, 1.7×10^{-13}–1.3×10^{-12} cm^3 molecule^{-1} s^{-1}.

Figure 4(d) compares bay-capping rate constants for various systems calculated earlier by us [10,15-17] and in the present work at the same level of theory, including the acetylene addition reactions to σ radicals incorporating two six-membered rings connected by a C-C bond (biphenylyl), with a central six-membered ring (4-phenanthrenyl), with a central five-membered ring (7-fluoranthenyl and benzo[*ghi*]fluoranthen-5-yl), one six- and one five-membered ring ($C_{21}H_{11}$ R2), and two five-membered rings ($C_{20}H_9$). All these reactions are fast, with rate constants at 1500 K in the 8.9×10^{-13}–7.5×10^{-12} cm^3 molecule^{-1} s^{-1} range. The kinetics in the forward direction is controlled by the entrance barrier, the lowest for $C_{20}H_9$ (1.4 kcal/mol) and the highest for 4-phenanthrenyl (4.7 kcal/mol), and the branching between the bay-capping pathway and the formation of the ethynyl-substituted reactant. In the meantime, the enthalpy of the bay-capping process determines the rate of the reverse reaction of acetylene desorption, slowest for biphenylyl (phenanthrene + H) and 4-phenanthrenyl (pyrene + H) and fastest for $C_{20}H_9$ (indaceno[2,1,8,7-*cdefg*]pyrene + H).

3.3 Kinetic Monte Carlo simulations of PAH growth

The site-specific rate constants for the bay-capping reactions were tested in kMC simulations of the PAH growth. The kMC simulations followed evolution of naphthalene in a sooting-flame environment of an atmospheric burner-stabilized flames of ethylene, specifically, a stagnation 16.3% C_2H_4–23.7% O_2–Ar flame of Wang and co-workers [42] (cold gas velocity 8.0 cm/s and burner-to-stagnation surface separation 0.8 cm). The flame was computed with the FFCM1 model [43] using Cantera [44].

The stochastic evolution of PAH structure was simulated using the Gillespie algorithm [45] with an updated kMC model [20,46]. The reaction rate constants were calculated using the time-dependent temperature and gaseous species profiles (H, H_2, C_2H_2, CH_3, O, OH, O_2) obtained in the flame simulations. The rate-constant values were updated every10 μs.

Most of the starting naphthalene molecules were oxidized and/or thermally decomposed; hence 50,000 runs were carried out for each case to collect sufficient statistics of molecular evolution.

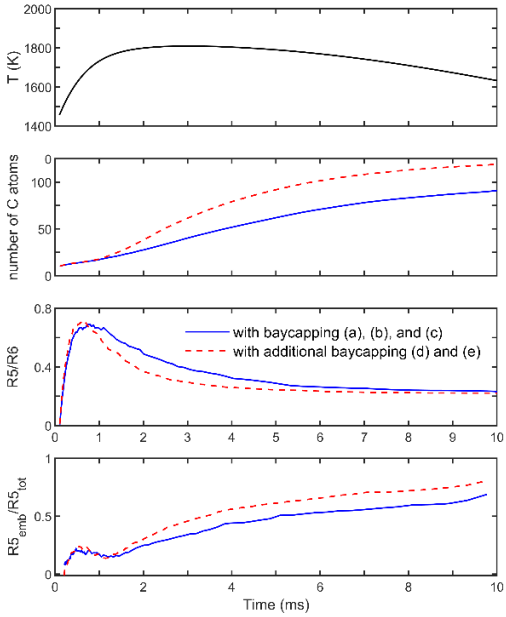

Fig. 5. Top panel: flame temperature profile. Bottom three panels: numerical results of kMC simulations with 6-0-6, 6-6-6, and 6-5-6 bay site capping only (blue) and with new capping reactions at bays 6-6-5 and 5-6-5 added (red) per evolving molecular structure, second panel from the top:

the number of carbon atoms, third panel: ratio of the five- to six membered rings, bottom panel: fraction of the embedded five-membered rings.

The results of the kMC simulations are presented in Fig. 5, comparing the cases with and without inclusion of the new capping reactions. Overall, the numerical results indicate that the additional capping reactions, namely those at the 6-6-5 and 5-6-5 sites, are frequent enough to affect measurably the PAH evolution.

A closer examination of the computed trends indicates that the inclusion of the additional capping increases, as expected, the rate of growth, which can be observed in the second panel of Fig. 5. Yet, perhaps somewhat unexpectedly, the fraction of five-membered rings is reduced, not increased, which is noticeable in the third panel of Fig. 5.

This result, however, become understood by noticing that the capping of sites 6-6-5 and 5-6-5 results in the formation of semi-embedded five-membered rings, which are less reactive to both growth [47] and oxidation [46]. In the present simulations, these sites were primarily converted to six-member rings in reactions with CH_3 and to a lesser extent to embedded five-member rings in bay-capping reactions with C_2H_2. This, in turn, reduced the presence of five-membered rings at the PAH edge.

Thus, while the total fraction of the five-membered rings is decreased with the additional bay capping, the number of embedded five-membered rings is increased, as shown in the bottom panel of Fig. 5. The latter observation is also consistent with the increase in closed-shell PAH formation, from 2 to 13 %, with the inclusion of capping at 6-6-5 and 5-6-5 bays.

4. Conclusions

We explored the bay-capping mechanism and kinetics via acetylene addition reactions to the 6-6-5 and 5-6-5 bays modeled by $C_{21}H_{11}$ and $C_{20}H_9$ radicals. The $C_{20}H_9 + C_2H_2$ reaction features a low entrance barrier and rapidly forms the bay-capped product, along with the ethynyl substituted reactant at temperatures above 1400 K. The reactivity of $C_{21}H_{11}$ is determined by the location of the unpaired electron; the π radical, R1, formed by H abstraction from the CH_2 group in $C_{21}H_{12}$ reacts with C_2H_2 very slowly owing to a high entrance barrier. The bay-capping rate constant for R1 approaches 10^{-16} cm^3 molecule^{-1} s^{-1} only at temperatures above 2000 K. Thus, the growth of π aryl radicals via acetylene addition is inefficient, which reflects the generally low reactivity of such radicals where the spin density is highly delocalized over the entire polyaromatic system; low reactivity of π radicals toward C_2H_2 addition contrasting them from σ radicals is anticipated to be a common feature in PAH growth. The σ $C_{21}H_{11}$ radical, R2, produced by H abstraction from the five-membered ring at the bay reacts rapidly with C_2H_2 forming the bay-capped product with the rate constant on the order of 10^{-12} cm^3 molecule^{-1} s^{-1} at $T \geq 1500$ K. Rate expressions for the capping reactions at the 6-6-5 and 5-6-5 bays are generated (Table 1 and Supplementary Material) and the rate constants are compared with those at the 6-0-6, 6-6-6, and 6-5-6 bays. kMC simulations of the PAH growth utilizing the site-specific bay-capping rate constants showed measurable differences when the 6-6-5 and 5-6-5 bay-capping reactions are taken into account, including an increase of the total growth rate and a rise of the number of embedded five-membered rings, with a slight decrease of their overall amount.

Table 1
Parameters of fitted modified Arrhenius expressions $k = A_1\, T^{\alpha_1} \exp(-E_a^1/RT) + A_2\, T^{\alpha_2} \exp(-E_a^2/RT)$ at 1 atm. A are in cm^3 mol^{-1} s^{-1} or s^{-1} and E_a in cal mol^{-1}.

	A	α	E_a	T range
$C_{20}H_9 + C_2H_2$ (R) →				
p1 + H	2.46E+66	-14.473	54446	500-2500
	2.12E+20	-1.6145	21332	
p2 + H	2.68E+74	-16.886	55985	500-2500
	1.30E+96	-25.45	49262	
$C_{22}H_{10}$ (**p1**) + H →				
R	4.62E+73	-16.14	70699	500-2500
	1.97E+27	-3.1857	37461	
p2 + H	3.92E+99	-23.889	78209	500-2500
	2.01E+44	-8.5029	40508	
$C_{22}H_{10}$ (**p2**) + H →				
R	1.01E+83	-18.308	83190	500-2500
	1.37E+102	-26.087	75392	
p1 + H	7.33E+100	-23.636	89111	500-2500
	1.82E+45	-8.1741	51131	
$C_{21}H_{11}$ (R2) + C_2H_2 →				
i14	2.91E+89	-21.27	64964	500-2000
	2.06E+23	-3.1638	8287.7	
p4 + H	4.56E+21	-2.1527	31220	500-2500
	7.97E+82	-18.585	84882	
p9 + H	3.35E-08	6.3571	21568	500-2500
	8.13E+81	-17.782	98888	
$C_{23}H_{13}$ (**i14**) →				
p4 + H	6.09E+85	-20.354	109340	500-2000
	3.19E+28	-4.3469	71248	
p9 + H	1.12E+64	-13.714	114160	500-2000
	3.56E+23	-2.7323	77567	
$C_{23}H_{12}$ (**p4**) + H →				
p5 +	8.92E+45	-8.5138	34082	700-2500

H				
$C_{23}H_{12}$ (**p9**) + H →				
i14	23.363	3.9052	-1247.5	500-1750
	-1.51E+32	-4.3886	30259	
p4 + H	3.25E+38	-6.4724	39050	500-2500
	5.71E+107	-25.371	95481	

Acknowledgements

The work was supported by the US Department of Energy, Basic Energy Sciences DE-FG02-04ER15570 to the Florida International University. We acknowledge the Instructional & Research Computing Center (IRCC, web: http://ircc.fiu.edu) at FIU and the National Energy Research Scientific Computing Center (NERSC) of the Office of Science in the U.S. Department of Energy for providing computing resources.

References

[1] M. Frenklach, D.W. Clary, W.C. Gardiner, S.E. Stein, Detailed kinetic modeling of soot formation on shock-tube pyrolysis of acetylene, *Symp. (Int.) Combust.* 20 (1984) 887-901.

[2] M. Frenklach and H. Wang, Detailed modeling of soot particle nucleation and growth, *Symp. (Int.) Combust.* 23 (1991) 1559-1566.

[3] M. Frenklach, D.W. Clary, W.C. Gardiner Jr., S.E. Stein, Effect of fuel structure on pathways to soot, *Proc. Combust. Inst.* 21 (1988) 1067-1076.

[4] M. Frenklach, T. Yuan, M. K. Ramachandra, Soot formation in binary hydrocarbon mixtures. *Energy Fuels* 2 (1988) 462-480.

[5] H. Richter, W.J. Grieco, J.B. Howard, Formation mechanism of polycyclic aromatic hydrocarbons and fullerenes in premixed benzene flames, *Combust. Flame* 119 (1999) 1-22.

[6] J. Appel, H. Bockhorn, M. Frenklach, Kinetic modeling of soot formation with detailed chemistry and physics: Laminar premixed flames of C-2 hydrocarbons, *Combust. Flame* 121 (2000) 122-136.

[7] A. Ciajolo, A. Tregrossi, M. Mallardo, T. Faravelli, E. Ranzi, Experimental and kinetic modeling study of sooting atmospheric-pressure cyclohexane flame, *Proc. Combust. Inst.* 32 (2009) 585-591.

[8] C. Marchal, J.L. Delfau, C. Vovelle, G. Moreac, C. Mounaim-Rousselle, F. Mauss, Modelling of aromatics and soot formation from large fuel molecules, *Proc. Combust. Inst.* 32 (2009) 753-759.

[9] C. Saggese, S. Ferrario, J. Camacho, A. Cuoci, A. Frassoldati, E. Ranzi, H. Wang, T. Faravelli, Kinetic modeling of particle size distribution of soot in a premixed burner-stabilized stagnation ethylene flame, *Combust. Flame* 162 (2015) 3356-3369.

[10] M. Frenklach, R.I. Singh, A.M. Mebel, On the low-temperature limit of HACA, *Proc. Combust. Inst.* 37 (2019) 969-976.

[11] D.S.N. Parker, R.I. Kaiser, T.P. Troy, M. Ahmed, Hydrogen abstraction/acetylene addition revealed, *Angew. Chem., Int. Ed.* 53 (2014) 7740-7744.

[12] T. Yang, T.P. Troy, B. Xu, O. Kostko, M. Ahmed, A.M. Mebel, R.I. Kaiser, Hydrogen-abstraction/acetylene-addition exposed, *Angew. Chem., Int. Ed.* 55 (2016) 14983-14987.

[13] T.-C. Chu, Z.J. Buras, M.C. Smith, A.B. Uwagwu, W.H. Green, From benzene to naphthalene: direct measurement of reactions and intermediates of phenyl radicals and acetylene, *Phys. Chem. Chem. Phys.* 21 (2019) 22248-22258.

[14] X. You, R. Whitesides, D. Zubarev, W.A. Lester Jr, M. Frenklach, Bay-capping reactions: kinetics and influence on graphene-edge growth, Proc. Combust. Inst. 33 (2011) 685–692.

[15] T. Yang, R.I. Kaiser, T.P. Troy, B. Xu, O. Kostko, M. Ahmed, A.M. Mebel, M.V. Zagidullin, V.N. Azyazov, HACA's heritage: A free-radical pathway to phenanthrene in circumstellar envelopes of asymptotic giant branch stars, *Angew. Chem., Int. Ed.* 56 (2017) 4515-4519.

[16] L. Zhao, R.I. Kaiser, B. Xu, U. Ablikim, M. Ahmed, D. Joshi, G. Veber, F.R. Fischer, A.M. Mebel, Pyrene synthesis in circumstellar envelopes and its role in the formation of 2D nanostructures, *Nat. Astron.* 2 (2018) 413-419.

[17] L. Zhao, S. Doddipatla, R.I. Kaiser, W. Lu, O. Kostko, M. Ahmed, L.B. Tuli, A.N. Morozov, A.H. Howlader, S.F. Wnuk, A.M. Mebel, V.N. Azyazov, R.K. Mohamed, F.R. Fischer, Gas phase synthesis of corannulene – a molecular building block of fullerenes – in circumstellar envelopes, *Phys. Chem. Chem. Phys.* 23 (2021) 5740-5749.

[18] H. Kroto, The stability of the fullerenes C_n, with n = 24, 28, 32, 36, 50, 60 and 70. *Nature* 329 (1987) 529–531.

[19] R. Whitesides, D. Domin, R. Salomón-Ferrer, W.A. Lester Jr, M. Frenklach, Embedded-ring migration on graphene zigzag edge, *Proc. Combust. Inst.* 32 (2009) 577–583.

[20] R. Whitesides, M. Frenklach, Detailed kinetic Monte Carlo simulations of graphene-edge growth, *J. Phys. Chem. A* 114 (2010) 689–703.

[21] E.K.Y. Yapp, C.G. Wells, J. Akroyd, S. Mosbach, R. Xu, M. Kraft, Modelling PAH curvature in laminar premixed flames using a detailed population balance model, *Combust. Flame* 176 (2017) 172-180.

[22] F. Schulz, M. Commodo, K. Kaiser, G. De Falco, P. Minutolo, G. Meyer, A. D'Anna, L. Gross, Insights into incipient soot formation by atomic force microscopy, *Proc. Combust. Inst.* 37 (2018) 885-892.

[23] K.O. Johansson, T. Dillstrom, P. Elvati, M.F. Campbell, P.E. Schrader, D.M. Popolan-Vaida, N.K. Richards-Henderson, K.R. Wilson, A. Violi, H.A. Michelsen, Radical–radical reactions, pyrene nucleation, and incipient soot formation in combustion, *Proc. Combust. Inst.* 36 (2017) 799–806.

[24] X. Shi, Q. Wang, A. Violi, Reaction pathways for the formation of five-membered rings onto polyaromatic hydrocarbon framework, *Fuel* 283 (2021) 119023.

[25] G. Leon, A. Menon, L. Pascazio, E.J. Bringley, J. Akroyd, M. Kraft, Kinetic Monte Carlo statistics of curvature integration by HACA growth and bay closure reactions for PAH growth in a counterflow diffusion flame, *Proc. Combust. Inst.* 38 (2021) 1449-1457.

[26] A.D. Becke, Density-functional thermochemistry. III. The role of exact exchange, *J. Chem. Phys.* 98 (1993) 5648–5652.

[27] Lee, W. Yang, R.G. Parr, Development of the Colle-Salvetti correlation-energy formula into a functional of the electron density. *Phys. Rev. B* 37 (1988) 785–789.

[28] A.G. Baboul, L.A. Curtiss, P.C. Redfern, K. Raghavachari, Gaussian-3 theory using density functional geometries and zero-point energies, *J. Chem. Phys.* 110 (1999) 7650–7657.

[29] L.A. Curtiss, K. Raghavachari, P.C. Redfern, A.G. Baboul, J.A. Pople, Gaussian-3 theory using coupled cluster energies, *Chem. Phys. Lett.* 314 (1999) 101–107.

[30] M.J. Frisch, G.W. Trucks, H.B. Schlegel, G.E. Scuseria, M.A. Robb, J.R. Cheeseman, G. Scalmani, V. Barone, G.A. Petersson, H. Nakatsuji, et al. *Gaussian 16, Revision C.01*; Gaussian, Inc.: Wallingford, CT, 2019.

[31] H.-J. Werner, P.J. Knowles, G. Knizia, F.R. Manby, M. Schütz, and others, *MOLPRO, version 2021.2*, a package of ab initio programs, see https://www.molpro.net.

[32] A. Fernandez-Ramos, J.A. Miller, S.J. Klippenstein, D.G. Truhlar, Modeling the kinetics of bimolecular reactions, *Chem. Rev.* 106 (2006) 4518-4584.

[33] Y. Georgievskii, J.A. Miller, M.P. Burke, S.J. Klippenstein, Reformulation and solution of the master equation for multiple-well chemical reactions, *J. Phys. Chem. A* 117 (2013) 12146–12154.

[34] Y. Georgievskii, S.J. Klippenstein, Master equation system solver (MESS), 2015, available at https://tcg.cse.anl.gov/papr/.

[35] H. Wang, M. Frenklach, Transport properties of polycyclic aromatic hydrocarbons for flame modeling, *Combust. Flame* 96 (1994) 163–170.

[36] Vishnyakov, P.G. Debenedetti, A.V. Neimark, Statistical geometry of cavities in a metastable confined fluid, *Phys. Rev. E* 62 (2000) 538-544.

[37] A.V. Neimark, P.I. Ravikovitch, A. Vishnyakov, Adsorption hysteresis in nanopores, *Phys. Rev. E* 62 (2000) 1493-1496.

[38] J. Troe, Theory of thermal unimolecular reactions at low pressures. I. Solutions of the master equation, *J. Chem. Phys.* 66 (1977) 4745–4757.

[39] A.W. Jasper, C.M. Oana, J.A. Miller, Third-body collision efficiencies from combustion modeling: Hydrocarbons in atomic and diatomic baths. *Proc. Combust. Inst.* 35 (2015) 197-204.

[40] A.M. Mebel, Y. Georgievskii, A.W. Jasper, S.J. Klippenstein, Temperature- and pressure-dependent rate coefficients for the HACA pathways from benzene to naphthalene, *Proc. Combust. Inst.* 36 (2017) 919-926.

[41] A.M. Mebel, Y. Georgievskii, A.W. Jasper, S.J. Klippenstein, Pressure-dependent rate constants for PAH growth: formation of indene and its conversion to naphthalene, *Faraday Discuss.* 195 (2016) 637-670.

[42] A.D. Abid, J. Camacho, D.A. Sheen, H. Wang, Quantitative measurement of soot particle size distribution in premixed flames—The burner-stabilized stagnation flame approach, *Combust. Flame* 156 (2009) 1862-1870.

[43] G.P. Smith, Y. Tao, H. Wang, Foundational fuel chemistry model Version 1.0 (FFCM-1), 2016. http://nanoenergy.stanford.edu/ffcm1.

[44] D.G. Goodwin, R.L. Speth, H.K. Moffat, B.W. Weber, Cantera: An object-oriented software toolkit for chemical kinetics, thermodynamics, and transport processes. https://cantera.org/. 2021.

[45] D.T. Gillespie, Exact stochastic simulation of coupled chemical reactions, *J. Phys. Chem.* 81 (1977) 2340-2361.

[46] M. Frenklach, Z. Liu, R.I. Singh, G.R. Galimova, V.N. Azyazov, A.M. Mebel, Detailed, sterically-resolved modeling of soot oxidation: role of O atoms, interplay with particle nanostructure, and emergence of inner particle burning, *Combust. Flame* 188 (2018) 284-306.

[47] A.S. Semenikhin, A.S. Savchenkova, I.V. Chechet, S.G. Matveev, M. Frenklach, A.M. Mebel, Transformation of an embedded five-membered ring in polycyclic aromatic hydrocarbons via the hydrogen-abstraction–acetylene-addition mechanism: A theoretical study, *J. Phys. Chem. A* 125 (2021) 3341-3354.